14062023

Label-free imaging of DNA interactions with 2D materials

Jenny Sülzle[1,*], Wayne Yang[2,*,†], Yuta Shimoda[2], Nathan Ronceray[2], Eveline Mayner[2] , Suliana Manley[1,†], and Aleksandra Radenovic[2,†]

[1] Institute of Physics and Institute of Bioengineering, Laboratory of Experimental Biophysics (LEB), École Polytechnique Fédérale de Lausanne (EPFL), Switzerland

[2] Institute of Bioengineering, Laboratory of Nanoscale Biology (LBEN), École Polytechnique Fédérale de Lausanne (EPFL), Switzerland

* Equal contribution

[†] Corresponding authors:

aleksandra.radenovic@epfl.ch; suliana.manley@epfl.ch; wayne.yang@epfl.ch

Abstract:

Two-dimensional (2D) materials offer potential as substrates for biosensing devices, as their properties can be engineered to tune interactions between the surface and biomolecules. Yet, not many methods can measure these interactions in a liquid environment without introducing labeling agents such as fluorophores. In this work, we harness interferometric scattering (iSCAT) microscopy, a label-free imaging technique, to investigate the interactions of single molecules of long dsDNA with 2D materials. The millisecond temporal resolution of iSCAT allows us to capture the transient interactions and to observe the dynamics of unlabeled DNA binding to a hexagonal boron nitride (hBN) surface in solution for extended periods (including a fraction of 6%, of trajectories lasting longer than 100 ms). Using a Focused Ion Beam (FIB) technique to engineer defects, we find that DNA binding affinity is enhanced at defects; when exposed to long lanes, DNA binds preferentially at lane edges. Overall, we demonstrate that iSCAT imaging is a useful tool to study how biomolecules interact with 2D materials, a key component in engineering future biosensors.

Keywords: DNA-surface interactions, interferometric scattering, 2D materials, biosensing

Two-dimensional (2D) materials have been developed as DNA sensing platforms owing to their chemical, electronic and mechanical properties which accommodate a variety of sensing modalities such as membrane-embedded nanopores[1–7], tunneling junctions[8,9] and field-effect transistors[10,11]. Such devices have succeeded in sensing individual DNA strands, both optically and electronically[12–16]. Different sensing modalities and functionalisations can be integrated to detect a whole host of biological analytes with a single device, which due to a high surface-to-volume ratio can be performed on limited sample volumes.

An important remaining challenge is to control surface interactions and to prevent fouling of the devices[17]. Toward this end, understanding DNA interactions with 2D materials is crucial to improve biosensor designs by reducing unwanted interactions and by promoting desired ones. A common approach is to label DNA fluorescently with intercalating dyes (such as YOYO-1) and study it with optical microscopy[18]. Alternatively, atomic force microscopy (AFM) can simultaneously detect molecular binding and map the surfaces[19,20]. Electron microscopy (EM) has also been used to image 2D materials in the presence of biomolecules at even higher spatial resolution[21–23]. However, each of these approaches suffers from limitations. Intercalating dyes change the length and stiffness of DNA[24,25], and such dyes suffer from photobleaching and quenching near 2D material surfaces[26,27]. AFM offers imaging in liquid, but only for hydrophilic substrates such as mica. In the case of prototypical 2D materials, such as graphene, hexagonal boron nitride (hBN) or transition metal dichalcogenides (TMDCs), imaging is often limited to dried DNA on 2D material surfaces. EM is largely confined to dry specimens and thus lacks dynamic information, or requires special liquid holders or the use of gold nanoparticles as labels[28–32]. This may explain in part why simulation has led experiment in investigating interactions of DNA with more complex materials and device designs[33–36].

In this work we harness interferometric scattering (iSCAT) microscopy[37,38] to investigate single molecules of long double stranded (ds)DNA interacting with the surface of hBN. As an analyte in solution approaches the surface, interference between the light it scatters and the light reflected by

53 the liquid-solid interface boosts the signal contrast, enabling single-molecule detection. Because iSCAT
54 uses the molecules themselves to generate signal, it does not require labeling, down to molecular
55 weights of 10 kDa for proteins[39]. Liberated from the limited photon budget of fluorescent dyes, the
56 technique allows millisecond temporal resolution, and theoretically indefinite imaging times. So far,
57 iSCAT has been used to study the mass distribution of short ssDNA[40], protein oligomerization[41], and
58 other biomolecular reactions[42] as well as more complex cellular processes in 3D[43]. To study the effects
59 of surface properties on DNA binding, we study its interactions with pristine hBN as well as engineered
60 defects and nanostructures[44].

61 We chose hBN as our substrate due to its optical transparency (because of its band gap of 6
62 eV)[45] and potential for future engineering[33]. hBN was exfoliated on coverslips and imaged with iSCAT
63 (Figure 1a, SI Experimental Section). The hBN flakes show a static uniform scattering background when
64 illuminated in water, with stronger scattering from their edges. To prevent edge scattering from
65 overwhelming the weaker signal from dsDNA, we imaged the larger flakes, and ensured they filled the
66 selected FOV (Figure S1). Furthermore, we use multiple frames to calculate a running averaged
67 scattering background and produce a differential contrast image. There are currently two main
68 strategies used in iSCAT for isolating the weak scattering signal of the particles from the strong
69 scattering background signal: normalization by a temporal mean-filtered background[41,46,47] or a
70 temporal median-filtered background[48,49].

71 Upon the addition of DNA, we observe the appearance of scattering blobs with bright and
72 dark regions in images following median-filtered background subtraction, for a range of different DNA
73 lengths (Figure 1b). Theoretical studies have shown that iSCAT is highly sensitive to the axial position
74 of scattering particles. Even nanometric changes can result in a contrast inversion in the temporally-
75 filtered images, due to constructive and destructive interference[50,51]. Previous studies typically
76 measured lower molecular weight biomolecules, which led to more homogeneous signals. In our case,

77 we image larger particles on layers of 2D materials with thicknesses varying by tens of nanometers.
78 We speculate that this is the origin of the complex signals we observe from dsDNA.

79 In time-lapse experiments, we qualitatively observe motion of the scattering blobs (Figure 1b,
80 Figure S2 and Movie S1). The signal contrast in the frames when a particle approaches or leaves the
81 surface is typically low, but it increases when particles move along the surface. We wished to quantify
82 this motion, but we noticed that the same molecule could change contrast, shape, and occupied area
83 from frame to frame. We speculate that this is due to changing 3D conformations of the dsDNA on the
84 hBN surface. Existing strategies for detection and localization such as thresholding and spot detection
85 yield poor efficiency due to this complex appearance - this motivated us to develop a customized
86 image analysis pipeline.

87 We developed an approach to segment and localize the particles for data with a temporal
88 median-filtered background normalization (Figure 2a, Figure S3). We use the absolute value of the
89 signal, to combine both constructive and destructive interference contributions to the signal. We
90 optimize the threshold to avoid false positives from the noisy background, while still detecting faint
91 signals. Each particle's contrast-weighted center of mass defines its location, which can be connected
92 in time to reconstruct trajectories (SI Experimental Section). We manually validated the automatically-
93 tracked results by checking each step in the pipeline for a randomly selected subset of particles.

94 On pristine hBN, we observe a wide range of trajectory geometries and lengths (Figure 2b).
95 We split them into two groups (Figure 2c): those that are shorter or equal to 110 ms (i.e. 10 frames,
96 340 out of 362 total trajectories) and those that are longer than 110 ms (22 out of 362 total
97 trajectories). We noticed a high number of single-frame trajectories (178 out of 362 total trajectories),
98 although most localizations belong to trajectories lasting at least two frames (818 out of 991 total
99 localizations). Single-frame binding events likely correspond to DNA interacting transiently with the
100 surface due to weak charge-mediated surface interactions. To test this idea, we varied the salt
101 concentration by adding 50 mM of KCl. Under this condition, there appears to be fewer binding events

102 per area and time (Movie S3). Transient binding events are expected to be short-lived, lasting only a
103 few milliseconds. Detecting these events with fluorescence microscopy would be challenging due to
104 their brief duration; however, with iSCAT microscopy, we were able to take advantage of its temporal
105 resolution to capture these events. Overall, the measured mean dwell time is 28.0 ± 3.1 ms for 20 kbp
106 dsDNA on pristine hBN (*N= 3 repeats, 10,000 frames each*). We noticed some particles diffusing out
107 of the measured FOV (3.4 µm x 3.4 µm), which would lead to a slight underestimate of dwell times.
108 The observed dynamic nature of the DNA trajectories suggests that interactions of dsDNA with the
109 hBN surface are transient, allowing molecules to adsorb temporarily on the surface, and diffuse
110 laterally before detaching and diffusing back into the bulk solution.

111 We hypothesized that it could be possible to influence the DNA binding kinetics by engineering
112 the surface with fabricated structures that host more defects and hence present more binding sites.
113 To test this idea, we turned to a recently developed surface engineering method[44] (Figure 3a, SI
114 Experimental Section). While the technique was first demonstrated to produce optical emitters, we
115 saw two potential advantages for our application: there may be minimal damage to the underlying
116 surface of hBN revealed after the water etching step is completed, and the controlled etching may
117 reduce background scattering of the patterned hBN surfaces and edges. As a demonstration, we
118 patterned an array of craters, and monitored the surface with AFM imaging (Figure 3b). The sample
119 was submerged in H_2O to etch away the patterned surface, and within 15 min craters started forming.
120 We continued imaging the sample until the depth of the craters stabilised at ~12 nm after about one
121 hour. We also etched lanes using the same process, 1 µm wide, 35 nm deep, and spaced 1 µm apart
122 (Figure 3c). To characterize our structures, we quantified the RMS roughness of the surface. The RMS
123 roughness along the trench of the lanes is 2 nm, while for a single lane it is even lower (0.3-0.5 nm)
124 and of the surrounding hBN flake is 1.8 nm (Figure S4).

125 To observe the effect of FIB milling on the DNA binding affinity, we performed iSCAT imaging
126 experiments on a single large square milled onto a flake. Similar FIB milling processes have yielded

127 increased densities of optically active emitters (up to 40x increase, Figure S5) in hBN indicating an
128 increase in defect sites. We reconstructed the trajectories of the DNA on the FIB-milled areas (Figure
129 4a). The DNA trajectories have a mean dwell time of 49.1 ± 3.9 ms (*N= 3 repeats, 10,000 frames each*,
130 Figure 4b, Figure S6). This is significantly larger than the previously observed dwell time of 28.0 ± 3.1
131 ms on the native flake. This indicates that there is an increased binding affinity, possibly from
132 interactions with the FIB milling induced defects on the hBN flake. The nanoscopic origins of these
133 interactions are still up for debate but a few hypotheses from molecular dynamics studies include
134 increased electrostatic interactions and reactivity with chemical species along the defect sites[36,52,53].

135 Next, we performed iSCAT imaging on an hBN patterned with narrow lanes as described above
136 (Figure 4c, Movie S2). The edges of the lanes offered scattering contrast, allowing us to contextualize
137 the binding of 20 kbp DNA to the surface. We observed an accumulation of DNA binding along the
138 edges of the etched lanes (x axis, Figure 4d, Figure S7). In contrast, along the direction of the lanes (y
139 axis), binding events appear uniformly distributed.

140 We wondered whether the preferential binding to lane edges would lead to anisotropic
141 trajectories, e.g. DNA particles preferentially moving along the lanes. For this we created polar plots
142 of trajectories (Figure S8), and decomposed mean squared displacement (MSD) and step size
143 distributions – along and perpendicular to the lanes (Figure S9, S10). The polar plots do not show a
144 preferential movement along one axis, including when considering only long trajectories. Similarly,
145 the MSD and step size distributions appeared isotropic.

146 In summary, we present a versatile method based on iSCAT for determining binding and dynamic
147 behavior of biomolecules on two-dimensional materials, in solution and without labels. We
148 demonstrate that iSCAT can distinguish the binding properties of different interfaces, beyond
149 detection of the mass of dsDNA. Additionally, the patterning of 2D material surfaces shows that it is
150 possible to engineer the interaction with dsDNA to create sites with increased interactions.
151 Surprisingly we did not observe directed motion of DNA along tracks. This calls for future exploration.

Furthermore, the data may contain more information about internal DNA configurations and dynamics, and we envision future analyses incorporating iSCAT PSF modeling will give more insights into these aspects. This method may accelerate the development of future biosensing devices that may harness engineered interactions to direct molecules towards sensing regions, such as the orifice of a nanopore, and improve the sensitivity of single molecule sensing.

Acknowledgments

W.Y. and A.R. would like to acknowledge funding from SNF grant CRSII5_193740. This work was supported by the National Centre for Competence in Research (NCCR) Chemical Biology (S.M., J.S.). We thank Lucie Navratilova for help and useful discussions on the plasma FIB milling. We acknowledge Michal Macha for the help with pFIB. We thank Kyle Douglass, the EPFL Hub for Image Analysis and Daniel Sage for their help and useful discussions on the image analysis workflow. We thank Nicolas Hundt for access to and support with the script for median-filtered iSCAT image processing.

Supporting information

Experimental section and figures as described in the text (PDF)

Supplementary Movie S1: Example of 20 kbp dsDNA on pristine hBN imaged with iSCAT (AVI)

Supplementary Movie S2: Example of 20 kbp dsDNA on FIB-milled hBN imaged with iSCAT (AVI)

Supplementary Movie S3: Example of 20 kbp dsDNA on pristine hBN in DI water and 50 mM KCl (AVI)

Author contribution

J.S., W.Y., S.M. and A.R. conceived the project and designed experiments. J.S., with assistance of W.Y., performed iSCAT imaging experiments. J.S. implemented the image processing framework and performed data analysis. W.Y. prepared the samples, carried out FIB milling, performed fluorescence imaging with the assistance of Y.S. and N.R. and carried out AFM measurements with assistance from E.M.. J.S., W.Y., S.M. and A.R. designed figures and wrote the manuscript.

References

(1) Merchant, C. A.; Healy, K.; Wanunu, M.; Ray, V.; Peterman, N.; Bartel, J.; Fischbein, M. D.; Venta, K.; Luo, Z.; Johnson, A. T. C.; Drndić, M. DNA Translocation through Graphene Nanopores. *Nano Lett.* **2010**, *10* (8), 2915–2921. https://doi.org/10.1021/nl101046t.

(2) Garaj, S.; Hubbard, W.; Reina, A.; Kong, J.; Branton, D.; Golovchenko, J. A. Graphene as a Subnanometre Trans-Electrode Membrane. *Nature* **2010**, *467* (7312), 190–193. https://doi.org/10.1038/nature09379.

(3) Verschueren, D. V.; Yang, W.; Dekker, C. Lithography-Based Fabrication of Nanopore Arrays in Freestanding SiN and Graphene Membranes. *Nanotechnology* **2018**, *29* (14), 145302. https://doi.org/10.1088/1361-6528/aaabce.

(4) Graf, M.; Lihter, M.; Thakur, M.; Georgiou, V.; Topolancik, J.; Ilic, B. R.; Liu, K.; Feng, J.; Astier, Y.; Radenovic, A. Fabrication and Practical Applications of Molybdenum Disulfide Nanopores. *Nat Protoc* **2019**, *14* (4), 1130–1168. https://doi.org/10.1038/s41596-019-0131-0.

(5) Schneider, G. F.; Kowalczyk, S. W.; Calado, V. E.; Pandraud, G.; Zandbergen, H. W.; Vandersypen, L. M. K.; Dekker, C. DNA Translocation through Graphene Nanopores. *Nano Lett.* **2010**, *10* (8), 3163–3167. https://doi.org/10.1021/nl102069z.

(6) Liu, K.; Pan, C.; Kuhn, A.; Nievergelt, A. P.; Fantner, G. E.; Milenkovic, O.; Radenovic, A. Detecting Topological Variations of DNA at Single-Molecule Level. *Nat Commun* **2019**, *10* (1), 3. https://doi.org/10.1038/s41467-018-07924-1.

(7) Danda, G.; Masih Das, P.; Chou, Y.-C.; Mlack, J. T.; Parkin, W. M.; Naylor, C. H.; Fujisawa, K.; Zhang, T.; Fulton, L. B.; Terrones, M.; Johnson, A. T. C.; Drndić, M. Monolayer WS2 Nanopores for DNA Translocation with Light-Adjustable Sizes. *ACS Nano* **2017**, *11* (2), 1937–1945. https://doi.org/10.1021/acsnano.6b08028.

(8) Caneva, S.; Gehring, P.; García-Suárez, V. M.; García-Fuente, A.; Stefani, D.; Olavarria-Contreras, I. J.; Ferrer, J.; Dekker, C.; van der Zant, H. S. J. Mechanically Controlled Quantum Interference in Graphene Break Junctions. *Nature Nanotech* **2018**, *13* (12), 1126–1131. https://doi.org/10.1038/s41565-018-0258-0.

(9) Huang, S.; He, J.; Chang, S.; Zhang, P.; Liang, F.; Li, S.; Tuchband, M.; Fuhrmann, A.; Ros, R.; Lindsay, S. Identifying Single Bases in a DNA Oligomer with Electron Tunnelling. *Nature Nanotech* **2010**, *5* (12), 868–873. https://doi.org/10.1038/nnano.2010.213.

(10) Heerema, S. J.; Dekker, C. Graphene Nanodevices for DNA Sequencing. *Nature Nanotech* **2016**, *11* (2), 127–136. https://doi.org/10.1038/nnano.2015.307.

(11) Girdhar, A.; Sathe, C.; Schulten, K.; Leburton, J.-P. Graphene Quantum Point Contact Transistor for DNA Sensing. *Proceedings of the National Academy of Sciences* **2013**, *110* (42), 16748–16753. https://doi.org/10.1073/pnas.1308885110.

(12) Yamazaki, H.; Kimura, S.; Tsukahara, M.; Esashika, K.; Saiki, T. Optical Detection of DNA Translocation through Silicon Nanopore by Ultraviolet Light. *Appl. Phys. A* **2014**, *115* (1), 53–56. https://doi.org/10.1007/s00339-013-7956-0.

(13) Soni, G. V.; Singer, A.; Yu, Z.; Sun, Y.; McNally, B.; Meller, A. Synchronous Optical and Electrical Detection of Biomolecules Traversing through Solid-State Nanopores. *Review of Scientific Instruments* **2010**, *81* (1), 014301. https://doi.org/10.1063/1.3277116.

(14) Assad, O. N.; Di Fiori, N.; Squires, A. H.; Meller, A. Two Color DNA Barcode Detection in Photoluminescence Suppressed Silicon Nitride Nanopores. *Nano Lett.* **2015**, *15* (1), 745–752. https://doi.org/10.1021/nl504459c.

(15) Yang, W.; Dekker, C. Single-Molecule Ionic and Optical Sensing with Nanoapertures. In *Single Molecule Sensing Beyond Fluorescence*; Bowen, W., Vollmer, F., Gordon, R., Eds.; Nanostructure Science and Technology; Springer International Publishing: Cham, 2022; pp 367–387. https://doi.org/10.1007/978-3-030-90339-8_12.

(16) Pitchford, W. H.; Kim, H.-J.; Ivanov, A. P.; Kim, H.-M.; Yu, J.-S.; Leatherbarrow, R. J.; Albrecht, T.; Kim, K.-B.; Edel, J. B. Synchronized Optical and Electronic Detection of Biomolecules Using a Low

Noise Nanopore Platform. *ACS Nano* **2015**, *9* (2), 1740–1748. https://doi.org/10.1021/nn506572r.

(17) Schneider, G. F.; Xu, Q.; Hage, S.; Luik, S.; Spoor, J. N. H.; Malladi, S.; Zandbergen, H.; Dekker, C. Tailoring the Hydrophobicity of Graphene for Its Use as Nanopores for DNA Translocation. *Nat Commun* **2013**, *4* (1), 2619. https://doi.org/10.1038/ncomms3619.

(18) Lu, C.; Liu, Y.; Ying, Y.; Liu, J. Comparison of MoS2, WS2, and Graphene Oxide for DNA Adsorption and Sensing. *Langmuir* **2017**, *33* (2), 630–637. https://doi.org/10.1021/acs.langmuir.6b04502.

(19) Pyne, A.; Thompson, R.; Leung, C.; Roy, D.; Hoogenboom, B. W. Single-Molecule Reconstruction of Oligonucleotide Secondary Structure by Atomic Force Microscopy. *Small* **2014**, *10* (16), 3257–3261. https://doi.org/10.1002/smll.201400265.

(20) Pyne, A. L. B.; Noy, A.; Main, K. H. S.; Velasco-Berrelleza, V.; Piperakis, M. M.; Mitchenall, L. A.; Cugliandolo, F. M.; Beton, J. G.; Stevenson, C. E. M.; Hoogenboom, B. W.; Bates, A. D.; Maxwell, A.; Harris, S. A. Base-Pair Resolution Analysis of the Effect of Supercoiling on DNA Flexibility and Major Groove Recognition by Triplex-Forming Oligonucleotides. *Nat Commun* **2021**, *12* (1), 1053. https://doi.org/10.1038/s41467-021-21243-y.

(21) Gentile, F.; Moretti, M.; Limongi, T.; Falqui, A.; Bertoni, G.; Scarpellini, A.; Santoriello, S.; Maragliano, L.; Proietti Zaccaria, R.; di Fabrizio, E. Direct Imaging of DNA Fibers: The Visage of Double Helix. *Nano Lett.* **2012**, *12* (12), 6453–6458. https://doi.org/10.1021/nl3039162.

(22) Zellweger, R.; Lopes, M. Dynamic Architecture of Eukaryotic DNA Replication Forks In Vivo, Visualized by Electron Microscopy. In *Genome Instability: Methods and Protocols*; Muzi-Falconi, M., Brown, G. W., Eds.; Methods in Molecular Biology; Springer: New York, NY, 2018; pp 261–294. https://doi.org/10.1007/978-1-4939-7306-4_19.

(23) Cerf, A.; Alava, T.; Barton, R. A.; Craighead, H. G. Transfer-Printing of Single DNA Molecule Arrays on Graphene for High-Resolution Electron Imaging and Analysis. *Nano Lett.* **2011**, *11* (10), 4232–4238. https://doi.org/10.1021/nl202219w.

(24) Günther, K.; Mertig, M.; Seidel, R. Mechanical and Structural Properties of YOYO-1 Complexed DNA. *Nucleic Acids Research* **2010**, *38* (19), 6526–6532. https://doi.org/10.1093/nar/gkq434.

(25) Rocha, M. S.; Ferreira, M. C.; Mesquita, O. N. Transition on the Entropic Elasticity of DNA Induced by Intercalating Molecules. *The Journal of Chemical Physics* **2007**, *127* (10), 105108. https://doi.org/10.1063/1.2768945.

(26) Tan, A. T. L.; Kim, J.; Huang, J.-K.; Li, L.-J.; Huang, J. Seeing Two-Dimensional Sheets on Arbitrary Substrates by Fluorescence Quenching Microscopy. *Small* **2013**, *9* (19), 3253–3258. https://doi.org/10.1002/smll.201300049.

(27) Kasry, A.; Ardakani, A. A.; Tulevski, G. S.; Menges, B.; Copel, M.; Vyklicky, L. Highly Efficient Fluorescence Quenching with Graphene. *J. Phys. Chem. C* **2012**, *116* (4), 2858–2862. https://doi.org/10.1021/jp207972f.

(28) Dunn, G.; Adiga, V. P.; Pham, T.; Bryant, C.; Horton-Bailey, D. J.; Belling, J. N.; LaFrance, B.; Jackson, J. A.; Barzegar, H. R.; Yuk, J. M.; Aloni, S.; Crommie, M. F.; Zettl, A. Graphene-Sealed Flow Cells for In Situ Transmission Electron Microscopy of Liquid Samples. *ACS Nano* **2020**, *14* (8), 9637–9643. https://doi.org/10.1021/acsnano.0c00431.

(29) Yuk, J. M.; Park, J.; Ercius, P.; Kim, K.; Hellebusch, D. J.; Crommie, M. F.; Lee, J. Y.; Zettl, A.; Alivisatos, A. P. High-Resolution EM of Colloidal Nanocrystal Growth Using Graphene Liquid Cells. *Science* **2012**, *336* (6077), 61–64. https://doi.org/10.1126/science.1217654.

(30) de Jonge, N.; Ross, F. M. Electron Microscopy of Specimens in Liquid. *Nature Nanotech* **2011**, *6* (11), 695–704. https://doi.org/10.1038/nnano.2011.161.

(31) Zheng, H.; Claridge, S. A.; Minor, A. M.; Alivisatos, A. P.; Dahmen, U. Nanocrystal Diffusion in a Liquid Thin Film Observed by in Situ Transmission Electron Microscopy. *Nano Lett.* **2009**, *9* (6), 2460–2465. https://doi.org/10.1021/nl9012369.

(32) Chen, Q.; Smith, J. M.; Park, J.; Kim, K.; Ho, D.; Rasool, H. I.; Zettl, A.; Alivisatos, A. P. 3D Motion of DNA-Au Nanoconjugates in Graphene Liquid Cell Electron Microscopy. *Nano Lett.* **2013**, *13* (9), 4556–4561. https://doi.org/10.1021/nl402694n.
(33) Zhang, L.; Wang, X. DNA Sequencing by Hexagonal Boron Nitride Nanopore: A Computational Study. *Nanomaterials* **2016**, *6* (6), 111. https://doi.org/10.3390/nano6060111.
(34) Manzanares-Palenzuela, C. L.; Pourrahimi, A. M.; Gonzalez-Julian, J.; Sofer, Z.; Pykal, M.; Otyepka, M.; Pumera, M. Interaction of Single- and Double-Stranded DNA with Multilayer MXene by Fluorescence Spectroscopy and Molecular Dynamics Simulations. *Chem. Sci.* **2019**, *10* (43), 10010–10017. https://doi.org/10.1039/C9SC03049B.
(35) Chen, S. H.; Bell, D. R.; Luan, B. Understanding Interactions between Biomolecules and Two-Dimensional Nanomaterials Using in Silico Microscopes. *Advanced Drug Delivery Reviews* **2022**, *186*, 114336. https://doi.org/10.1016/j.addr.2022.114336.
(36) Shankla, M.; Aksimentiev, A. Step-Defect Guided Delivery of DNA to a Graphene Nanopore. *Nat. Nanotechnol.* **2019**, *14* (9), 858–865. https://doi.org/10.1038/s41565-019-0514-y.
(37) Lindfors, K.; Kalkbrenner, T.; Stoller, P.; Sandoghdar, V. Detection and Spectroscopy of Gold Nanoparticles Using Supercontinuum White Light Confocal Microscopy. *Phys. Rev. Lett.* **2004**, *93* (3), 037401. https://doi.org/10.1103/PhysRevLett.93.037401.
(38) Jacobsen, V.; Stoller, P.; Brunner, C.; Vogel, V.; Sandoghdar, V. Interferometric Optical Detection and Tracking of Very Small Gold Nanoparticles at a Water-Glass Interface. *Opt. Express* **2006**, *14* (1), 405. https://doi.org/10.1364/OPEX.14.000405.
(39) Dahmardeh, M.; Mirzaalian Dastjerdi, H.; Mazal, H.; Köstler, H.; Sandoghdar, V. Self-Supervised Machine Learning Pushes the Sensitivity Limit in Label-Free Detection of Single Proteins below 10 KDa. *Nat Methods* **2023**, *20* (3), 442–447. https://doi.org/10.1038/s41592-023-01778-2.
(40) Li, Y.; Struwe, W. B.; Kukura, P. Single Molecule Mass Photometry of Nucleic Acids. *Nucleic Acids Research* **2020**, *48* (17), e97. https://doi.org/10.1093/nar/gkaa632.
(41) Young, G.; Hundt, N.; Cole, D.; Fineberg, A.; Andrecka, J.; Tyler, A.; Olerinyova, A.; Ansari, A.; Marklund, E. G.; Collier, M. P.; Chandler, S. A.; Tkachenko, O.; Allen, J.; Crispin, M.; Billington, N.; Takagi, Y.; Sellers, J. R.; Eichmann, C.; Selenko, P.; Frey, L.; Riek, R.; Galpin, M. R.; Struwe, W. B.; Benesch, J. L. P.; Kukura, P. Quantitative Mass Imaging of Single Biological Macromolecules. *Science* **2018**, *360* (6387), 423–427. https://doi.org/10.1126/science.aar5839.
(42) Hundt, N.; Cole, D.; Hantke, M. F.; Miller, J. J.; Struwe, W. B.; Kukura, P. Direct Observation of the Molecular Mechanism Underlying Protein Polymerization. *Science Advances* **2022**, *8* (35), eabm7935. https://doi.org/10.1126/sciadv.abm7935.
(43) Küppers, M.; Albrecht, D.; Kashkanova, A. D.; Lühr, J.; Sandoghdar, V. Confocal Interferometric Scattering Microscopy Reveals 3D Nanoscopic Structure and Dynamics in Live Cells. *Nat Commun* **2023**, *14* (1), 1962. https://doi.org/10.1038/s41467-023-37497-7.
(44) Glushkov, E.; Macha, M.; Räth, E.; Navikas, V.; Ronceray, N.; Cheon, C. Y.; Ahmed, A.; Avsar, A.; Watanabe, K.; Taniguchi, T.; Shorubalko, I.; Kis, A.; Fantner, G.; Radenovic, A. Engineering Optically Active Defects in Hexagonal Boron Nitride Using Focused Ion Beam and Water. *ACS Nano* **2022**, *16* (3), 3695–3703. https://doi.org/10.1021/acsnano.1c07086.
(45) Wickramaratne, D.; Weston, L.; Van de Walle, C. G. Monolayer to Bulk Properties of Hexagonal Boron Nitride. *J. Phys. Chem. C* **2018**, *122* (44), 25524–25529. https://doi.org/10.1021/acs.jpcc.8b09087.
(46) Piliarik, M.; Sandoghdar, V. Direct Optical Sensing of Single Unlabelled Proteins and Super-Resolution Imaging of Their Binding Sites. *Nat Commun* **2014**, *5* (1), 4495. https://doi.org/10.1038/ncomms5495.
(47) Cole, D.; Young, G.; Weigel, A.; Sebesta, A.; Kukura, P. Label-Free Single-Molecule Imaging with Numerical-Aperture-Shaped Interferometric Scattering Microscopy. *ACS Photonics* **2017**, *4* (2), 211–216. https://doi.org/10.1021/acsphotonics.6b00912.

(48) Heermann, T.; Steiert, F.; Ramm, B.; Hundt, N.; Schwille, P. Mass-Sensitive Particle Tracking to Elucidate the Membrane-Associated MinDE Reaction Cycle. *Nat Methods* **2021**, *18* (10), 1239–1246. https://doi.org/10.1038/s41592-021-01260-x.
(49) Foley, E. D. B.; Kushwah, M. S.; Young, G.; Kukura, P. Mass Photometry Enables Label-Free Tracking and Mass Measurement of Single Proteins on Lipid Bilayers. *Nat Methods* **2021**, *18* (10), 1247–1252. https://doi.org/10.1038/s41592-021-01261-w.
(50) Mahmoodabadi, R. G.; Taylor, R. W.; Kaller, M.; Spindler, S.; Mazaheri, M.; Kasaian, K.; Sandoghdar, V. Point Spread Function in Interferometric Scattering Microscopy (ISCAT). Part I: Aberrations in Defocusing and Axial Localization. *Opt. Express, OE* **2020**, *28* (18), 25969–25988. https://doi.org/10.1364/OE.401374.
(51) Dong, J.; Maestre, D.; Conrad-Billroth, C.; Juffmann, T. Fundamental Bounds on the Precision of ISCAT, COBRI and Dark-Field Microscopy for 3D Localization and Mass Photometry. *J. Phys. D: Appl. Phys.* **2021**, *54* (39), 394002. https://doi.org/10.1088/1361-6463/ac0f22.
(52) Ronceray, N.; You, Y.; Glushkov, E.; Lihter, M.; Rehl, B.; Chen, T.-H.; Nam, G.-H.; Watanabe, K.; Taniguchi, T.; Roke, S.; Keerthi, A.; Comtet, J.; Radha, B.; Radenovic, A. Liquid-Activated Quantum Emission from Native HBN Defects for Nanofluidic Sensing. arXiv December 12, 2022. https://doi.org/10.48550/arXiv.2204.06287.
(53) Balasubramanian, R.; Pal, S.; Rao, A.; Naik, A.; Chakraborty, B.; Maiti, P. K.; Varma, M. M. DNA Translocation through Vertically Stacked 2D Layers of Graphene and Hexagonal Boron Nitride Heterostructure Nanopore. *ACS Appl. Bio Mater.* **2021**, *4* (1), 451–461. https://doi.org/10.1021/acsabm.0c00929.

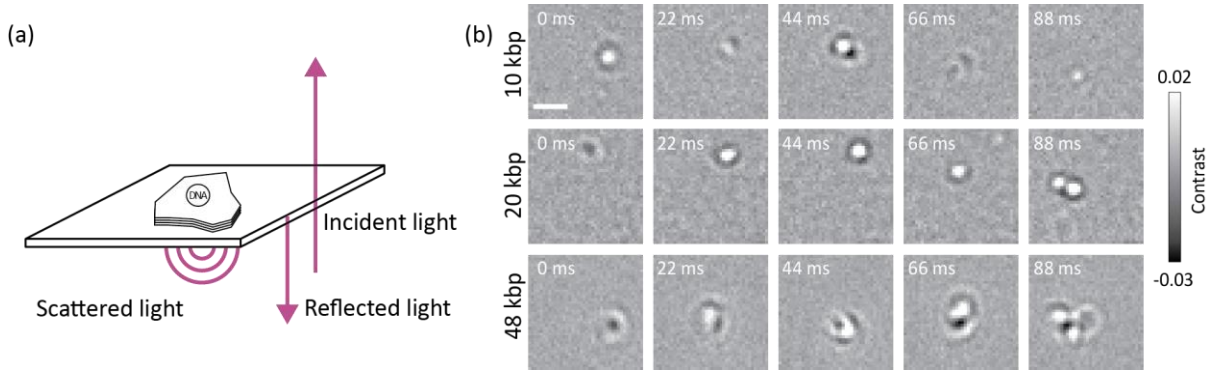

Figure 1. Interaction of 2D materials and DNA probed by iSCAT. (a) Schematic setup of the experiment. (b) Examples of median-filtered time series of 10, 20 and 48 kbp dsDNA particles arriving and diffusing on the hBN surface. Scale bar is 1 µm.

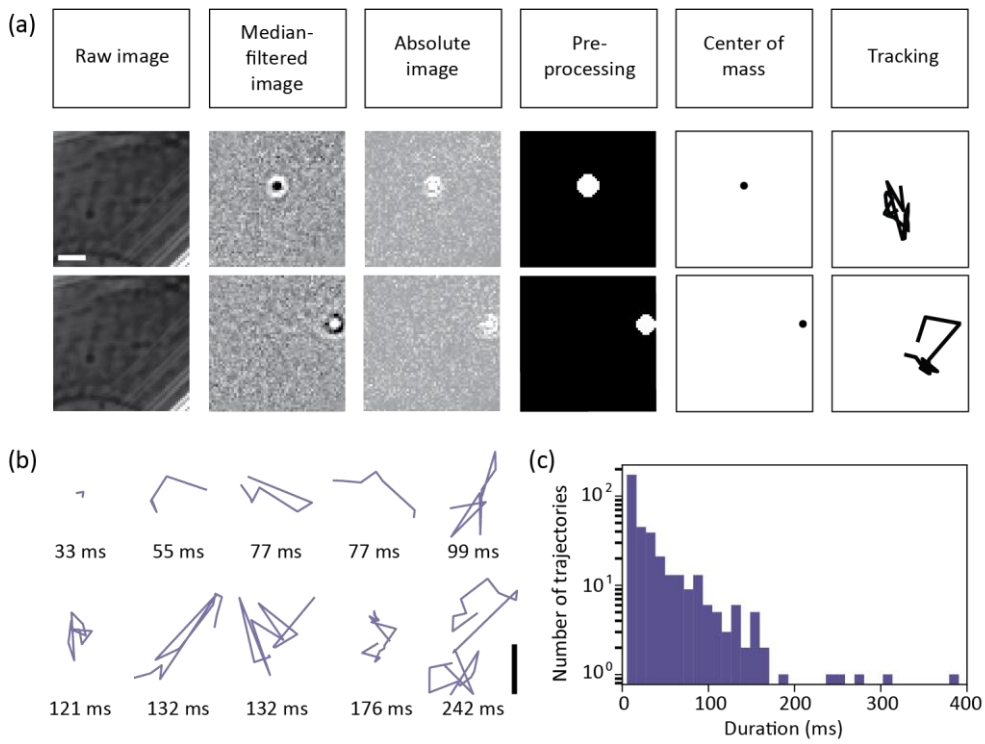

Figure 2. Overview of image processing workflow and of trajectories on pristine hBN. (a) Schematic of image processing workflow. (b) Examples of short and long trajectories on pristine hBN. (c) Dwell time of 20 kbp DNA on pristine hBN. The histogram represents all reconstructed trajectories from one representative measurement with 10,000 frames imaged at 90.5 Hz. N (total trajectories) = 362, N (L ≤ 110 ms) = 340, N (L > 110 ms) = 22. Data from replica measurements is provided in the SI. Scale bars are 1 µm.

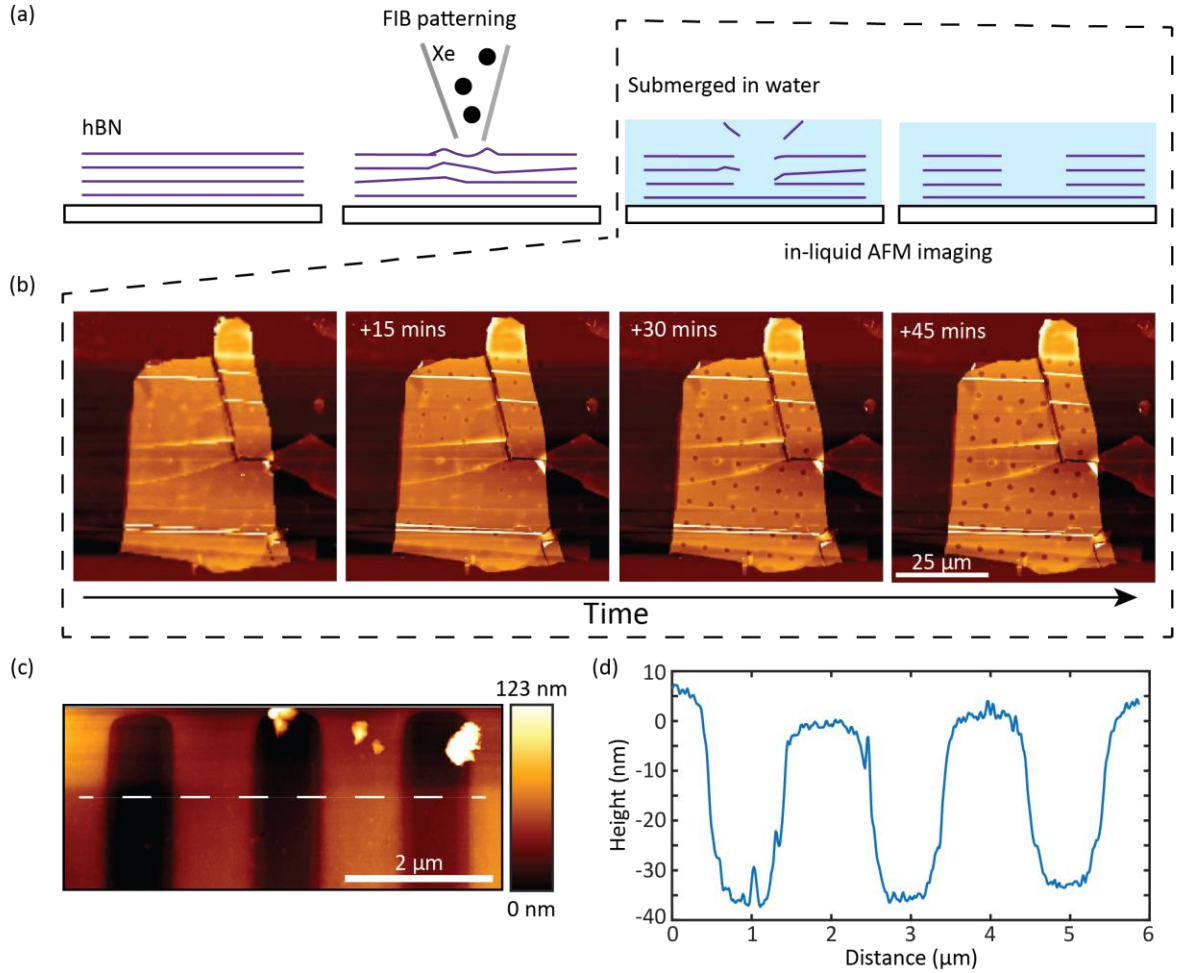

Figure 3. AFM image of pFIB-milled, water-assisted etching of hBN. (a) Illustration of the formation of hBN wells in H_2O. (b) Time series of a dot-patterned hBN flake upon immersion in water. (c) AFM surface map of tracks milled in hBN flake. (d) AFM height profile scan as indicated by the dashed line in (c), RMS roughness along the trench of the lanes is 2 nm.

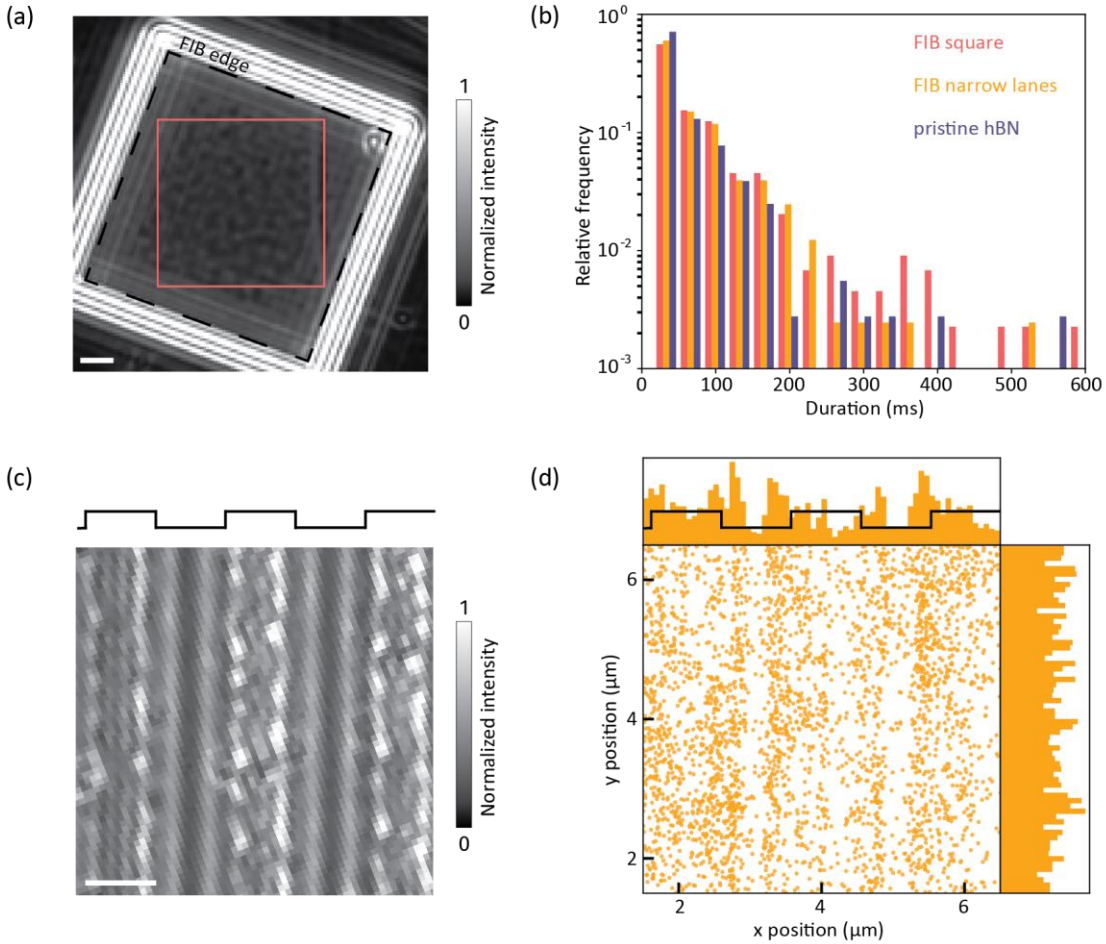

394

395 **Figure 4.** DNA interaction with FIB-milled hBN samples. (a) Native iSCAT image of an hBN flake with
396 an etched square (dashed line). Area used for quantitative analysis is highlighted in red. (b)
397 Comparison of dwell time of 20 kbp dsDNA on three different surfaces: hBN patterned with lanes,
398 pristine hBN and FIB-etched hBN (FIB square). The histogram represents all reconstructed trajectories
399 from three representative measurements with each 10,000 frames and 90.5 Hz frame rate, N (FIB
400 lanes) = 407, N (pristine hBN) = 362 and N (FIB square) = 561. (c) Native iSCAT image of an hBN flake
401 with etched lanes. (d) Distribution of binding spots of 20 kbp dsDNA on sample shown in (c). The
402 scatter histogram represents all binding spots from a representative measurement with 10,000 frames
403 and N = 1388. Scale bars are 1 µm.